

1 **Temporal considerations in the measurement of indoor mass**
2 **transfer coefficients**

3

4 Glenn C. Morrison, Deborah J. Wiseman

5 *Department of Civil, Architectural and Environmental Engineering*

6 *University of Missouri-Rolla, 221 Butler-Carlton Hall, Rolla, MO 65409-0030*

7

8 **Abstract**

9

10 Quantification of the transport of indoor pollutants to and from surfaces, key to
11 understanding indoor pollutant concentrations, can be highly inaccurate if the factors
12 causing the measured values to vary are not considered. Pollutant mass transport,
13 characterized by the “transport-limited deposition velocity”, v_t , is dynamic and
14 measurements of this mass-transfer coefficient can be influenced by changing conditions.
15 Through simulations we find that for large, but realistic, changes in indoor transport
16 conditions during the sampling period, time-averaged measurements of v_t can be in error
17 by 40% or more. Measurements using a highly surface reactive species, such as nitric
18 acid, incur the greatest error for infiltrated pollutants. The measurement error incurred for
19 species that are moderately surface reactive, such as ozone, varies depending on the type
20 of surfaces available for deposition. Further, the greater the variability in conditions, the
21 greater the error anticipated from time-averaged measurements of v_t .

22

23 *Keywords:* mass-transfer, pollutant transport, pollutant deposition, indoor air, temporal
24 measurement

25

26 **1. Introduction**

27

28 In the indoor environment, air pollution levels are driven by competition between
29 pollution sources and sinks. Indoor surfaces are extremely important as both sources and
30 sinks for pollutants. For example, emissions of sorbed volatile organic compounds
31 (VOCs) tend to drive VOC concentrations upward, whereas irreversible deposition of
32 ozone or SO₂ to surfaces drives indoor concentrations of these species downward.
33 Different materials, e.g. carpet vs. glass, emit or consume pollutants at different rates
34 depending on 1) surface composition and chemistry, 2) the geometry of that surface and
35 3) the rate that pollutants transport to or from that surface through the overlying fluid-
36 mechanical boundary layer. Through theoretical analyses of temporal variability, this
37 research estimates the magnitude of errors when measuring number (3), the rate of
38 transport through fluid-mechanical boundary layers over indoor surfaces.

39

40 *1.1 Deposition velocity and transport-limited deposition velocity*

41

42 Pollutant-specific indoor deposition rates are characterized by a mass-transfer
43 coefficient commonly referred to as the deposition velocity, v_d (Nazaroff et al., 1993).

44 The local, instantaneous flux, $J(s,t)$, at time t and at a point location s , to a surface is

$$45 \quad J(s,t) = v_d(s,t)C_b(s,t) \quad (1)$$

46 where $C_b(s,t)$ is the concentration at the outer edge of the concentration boundary layer.
47 Commonly, C_b is taken as the “core” concentration or the volume averaged room
48 concentration. Cano-Ruiz et al. (Cano-Ruiz et al., 1993) showed that $v_d(s,t)$ combines (a)
49 the resistance to transport through the fluid-mechanical boundary layer, and (b) the
50 resistance to uptake at the surface due to chemical or physical interactions:

$$51 \quad \frac{1}{v_d(s,t)} = \overset{(a)}{\left(\frac{1}{v_t(s,t)} \right)} + \overset{(b)}{\left(\frac{4}{\gamma(s,t) \langle v \rangle} \right)} \quad (2)$$

52 where $v_t(s,t)$ is the transport-limited deposition velocity (which applies to both deposition
53 and emission), $\gamma(s,t)$ is the probability that a pollutant will be consumed once it reaches
54 the surface and is known as the “reaction probability”, and $\langle v \rangle$ is Boltzman’s velocity for
55 the species. These sequential resistances to uptake are independent and therefore
56 independently quantifiable by measurement or by theoretical analyses. This conceptual
57 understanding of deposition can be expanded to include emissions from surfaces
58 (Morrison et al., 2003), where an overall mass-transfer coefficient combines the
59 resistance to surface-release of a pollutant and the resistance to transport across the
60 overlying fluid-mechanical boundary layer. For either deposition or emission, a key
61 parameter is the transport resistance across the boundary layer, which is independent of
62 the direction of net flux.

63 The transport-limited deposition velocity introduced in Eq (2) can be used directly
64 in the analysis of flux. The local flux in Eq (1), $J(s,t)$, to or from a surface is also given
65 by,

$$66 \quad J(s,t) = v_t(s,t)[C_b(s,t) - C_s(s,t)] \quad (3)$$

67 where $C_s(s,t)$ is the near-surface gas concentration of the pollutant. The magnitude of
68 $C_s(s,t)$ depends on dynamics taking place at the surface. For example, nitric acid
69 deposition to an indoor surface is nearly completely irreversible, and as a result $C_s(s,t)$ is
70 effectively zero. In contrast, for emission from a solvent spill, $C_s(s,t)$ is the saturation
71 concentration of the solvent.

72 Since surface fluxes of pollutants influence indoor air quality, it is desirable to
73 quantify the underlying parameters, such as $v_t(s,t)$, that control fluxes. The term $v_t(s,t)$ is
74 independent of concentrations for dilute systems. Instead $v_t(s,t)$ depends on the flow
75 conditions near the surface and the gaseous pollutant diffusivity. Thus $v_t(s,t)$ can be
76 determined from location specific measurement (Morrison et al., 2003) or model
77 calculations of flow conditions (Nazaroff and Cass, 1987).

78 *1.2 Measurement of indoor mass-transfer coefficients*

79 1.2.1 Measurements that rely on deposition

80 Nazaroff et al. (1993) explained that local flux measurements can be performed
81 by measuring the accumulated mass of a species on an appropriate surface. Several
82 measurements of this sort have been performed for radon progeny using alpha-particle
83 detection to determine accumulated mass, particles by direct mass accumulation and
84 nitric acid (Salmon et al., 1990) by accumulation of nitrate on a nylon filter. The reader
85 will find a review of these and other experiments and their results in Nazaroff et al.
86 (1993). More recently, the deposition flux of fluorescent particles (Thatcher and
87 Nazaroff, 1997), and ozone using the measured conversion of nitrite to nitrate on coated
88 filters (Morrison et al., 2003) has been quantified.

89 To measure $v_t(s,t)$, the majority of deposition experiments have relied on the fact
90 that the depositing species will not subsequently be emitted (irreversible uptake). Eq. (3)
91 can be simplified for each of these cases because the near-surface concentration is
92 approximately zero:

$$93 \quad J(s,t) = v_t(s,t)C_b(s,t) \quad (4)$$

94 This simplifies experiments because only the flux and the bulk concentration are required
95 to quantify v_t . Note that by comparing Eq. (4) to Eq (1), $v_t \sim v_d$ under these conditions.

96 It is useful at this point to briefly describe the DeVO method of (Morrison et al.,
97 2003), an example of a deposition-style measurement of $v_t(s,t)$ that will be referred to in
98 later discussions. In this method, ozone flux (J in Eq (4)) to a glass-fiber filter coated
99 with NaNO_2 is evaluated by quantifying the amount of nitrate ion formed over an 8 h
100 period by the reaction



102 The bulk concentration, C_b in Eq (4), is quantified with a photometric ozone analyzer.
103 Knowledge of J and C_b , can be used to obtain v_t , from Eq (4). Note, however, that Eq (4)
104 refers to local, s , and instantaneous, t , while the DeVO method evaluates J and C_b over an
105 area averaged by the size of the coated filter and averaged over the experimental time
106 period of 8 hours.

107 1.2.2 Measurements that rely on emissions

108 Although discussed above in terms of “deposition”, it should be understood that
109 emission experiments can also be used to measure v_t . The transport-limited deposition
110 velocity, v_t , is independent of net direction of flux and can be determined by emission
111 experiments as well as by deposition experiments. Volatile species such as solvents can

112 provide a measure of flux simply by measuring the rate of mass change of a coated
113 surface. For emissions, where the core room concentration is near zero,

114
$$J(s,t) = v_t(s,t)C_s(s,t) \quad (6)$$

115 Once again, experiments are simplified because only the flux and the near-surface
116 concentration are required. For pure species emission experiments, C_s is derived from the
117 vapor pressure. The DeVS device employed by Morrison et al. (2003) appears to be the
118 only example of emissions used to derive local and continuous indoor mass-transfer
119 coefficients.

120

121 **2. Theory: temporal dependence of transport**

122

123 To initiate this analysis, it is useful to clarify qualitatively and with examples why
124 temporal variability in transport conditions is important to consider in indoor modeling
125 and measurements. Nazaroff et al. (1993) evaluated the concept of deposition velocity
126 and concluded that the concept is valuable and appropriate to use in indoor air modeling.
127 However, they cautioned that deposition rates are strongly dependent on flow conditions
128 which will vary greatly among building types and ventilation and that using average
129 deposition velocities for a room or building may be inappropriate since the local values
130 may vary considerably. Adding to their cautions, it follows that deposition velocities may
131 vary not just in space but in time due to changes in activity, ventilation rates, and other
132 usage patterns in buildings. Thus, to improve the usefulness of the concept of deposition
133 velocity for indoor air quality modeling and exposure assessment, we require a better
134 understanding of the magnitude and variability of air/surface pollutant transport.

135

136 *2.1 Temporal variability in mass transport*

137

138 When considering the accuracy of transport measurements, temporal changes in
139 transport to or from surfaces may become important when time scales of change in
140 transport coincide with time scales for other phenomena. Commonly, non-steady state
141 models of indoor pollutants incorporate the assumption that the time scale for mixing (~
142 minutes) (Gadgil et al., 2003) is much faster than the average characteristic time for
143 concentration changes. In this way, mixing can be ignored and only the slower time
144 scales of ventilation (~ hours) or other phenomena are considered. However, time scales
145 for mixing may coincide with time scales for changes in transport rates. In considering
146 dynamic indoor concentrations of a pollutant, the instantaneous rate of change of the
147 volume-averaged bulk concentration is:

148
$$\frac{d\bar{C}_b(t)}{dt} = -\frac{1}{V} \int_s v_t(s,t)[C_b(s,t) - C_s(s,t)] ds \quad (7)$$

149 where V is volume. Because v_t and C_b are multiplied in the integral, coincident dynamics
150 of v_t and C_b preclude any attempt to consider them as independent parameters.

151 One example where these time scales may coincide is in a building with a window
152 open. A change in outdoor wind speed or direction will consequently change the rate of
153 natural ventilation through windows and simultaneously change the mixing
154 characteristics of the air within the building. For a sudden increase in air velocity through
155 a window into a room several phenomena change simultaneously. Indoor pollutants are
156 diluted or concentrated, while the energy of the moving air is dissipated by momentum
157 transfer to the rest of the air volume and to the walls. Since v_t is dependent on near-

158 surface air flow conditions, it is reasonable to assume that the rate of change in this mass-
159 transfer coefficient is roughly of the same order of magnitude as the rate of change of
160 mixing indoors. Therefore, the core concentration of the room likely is changing at nearly
161 the same rate as the surface mass-transfer coefficients.

162 Even over longer time-scales, assuming average conditions may not be prudent.
163 For example, ozone concentrations cycle daily with the sun. In a commercial building,
164 activity and ventilation also cycle daily. Thus, ozone concentrations and the intensity of
165 mixing and v_t would be coupled. The magnitude of error resulting from an artificial
166 separation of concentrations from transport parameters is unknown for indoor modeling.
167 An estimate of this error is derived and reported in the Results section for a simplified
168 indoor system.

169

170 *2.2 Dynamic vs time-averaged measurement of v_t*

171

172 Most methods used to determine deposition velocity have relied on long-term averages to
173 generate enough mass to discern a surface flux. For example, Salmon et al. (1990)
174 collected nitric acid on nylon covered plates for 10-12 weeks to obtain enough mass for
175 analysis. Morrison et al. (2003) typically required between 8 and 12 h to obtain sufficient
176 conversion of nitrite to nitrate to discern ozone flux to a coated filter.

177 Each of these methods is potentially flawed because they seek to quantify a time-
178 averaged value of the mass-transfer coefficient, \bar{v}_t or \bar{v}_d . As suggested in section 2.1,
179 this flaw arises because the measurement methods to arrive at \bar{v}_t and the definition of \bar{v}_t

180 are mismatched. The formal definition of \bar{v}_t at a specific location is the time integral of
181 the instantaneous deposition velocity, $v_t(s,t)$ divided by the time interval t_1 to t_2 :

$$182 \quad \bar{v}_t(s) = \frac{\int_{t_1}^{t_2} v_t(s,t) dt}{t_2 - t_1} \quad (8)$$

183

184 Also, by definition, instantaneous $v_t(s,t)$ derived using deposition as an example is

$$185 \quad v_t(s,t) = \frac{J(s,t)}{C_b(s,t)} \quad (9)$$

186 Therefore the *actual* time averaged ozone deposition velocity is

$$187 \quad \bar{v}_t(s) = \frac{\int_{t_1}^{t_2} \frac{J(s,t)}{C_b(s,t)} dt}{t_2 - t_1} = \overline{\left(\frac{J(s)}{C_b(s)} \right)} \quad (10)$$

188 However, because long periods of time are required to collect sufficient mass for an
189 average flux determination, it is generally impossible to evaluate the instantaneous flux
190 of a species to a collecting surface. Instead, Eq (10) is simplified to the following form
191 for want of a better way to determine $\bar{v}_t(s)$:

$$192 \quad \bar{v}_t(s) = \frac{\bar{J}(s)}{\bar{C}_b(s)} \quad (11)$$

193 where $\bar{J}(s)$ is the time averaged flux to the collecting surface and $\bar{C}_b(s)$ is the time-
194 averaged “bulk” air concentration (measured arbitrarily in the center of the room or at a
195 room air exhaust). For example, Morrison et al. (2003) reported the following equation
196 for determining the time-averaged, transport-limited deposition velocity for ozone, $\bar{v}_{t,ozone}$,
197 analysis of nitrite coated filters (the “DeVO” method):

198
$$\bar{v}_{t, \text{ozone}} = \frac{m_{\text{NO}_3} MW_{\text{O}_3}}{\bar{C}_{\text{O}_3} MW_{\text{NO}_3} A \Delta t} \quad (12)$$

199 where m_{NO_3} is the mass of nitrate formed on the filter (g), MW_{O_3} is the molecular weight
 200 of ozone (g mol^{-1}), MW_{NO_3} is the molecular weight of the nitrate ion (g mol^{-1}), \bar{C}_{O_3} is the
 201 time-averaged room concentration of ozone during the exposure interval ($\mu\text{g m}^{-3}$), A is
 202 the exposed area of the filter (m^2 or cm^2) and Δt is the time interval exposed (h or s). We

203 see that integrated molar flux of ozone is incorporated as $\left(\frac{m_{\text{NO}_3} MW_{\text{O}_3}}{MW_{\text{NO}_3} A \Delta t} \right)$. The time

204 averaged ozone concentration, \bar{C}_{O_3} , is evaluated separately (e.g. a UV-photometric ozone
 205 analyzer). Note that \bar{C}_{O_3} was not local as suggested in Eq. (11); a representative core
 206 concentration is usually substituted for the local concentration at the edge of the
 207 boundary layer. Thus for the a time-integrated method,

208
$$\bar{v}_t(s) = \frac{\bar{J}(s)}{\bar{C}_b(s)} = \frac{\int_{t_1}^{t_2} v_t(s,t) C_b(s,t) dt}{\int_{t_1}^{t_2} C_b(s,t) dt} \quad (13)$$

209 which is not equal to Eq. (10). Combining Eq. (10) and (13), Eq. (14) recapitulates the
 210 fact that the time-integrated flux methods result in only an approximation of the actual
 211 transport limited deposition velocity:

212
$$\frac{\bar{J}(s)}{\bar{C}_b(s)} \neq \overline{\left(\frac{J(s)}{C_b(s)} \right)}. \quad (14)$$

213 *2.3. Reporting metric for mass-transport*

214

215 Either deposition or emission may be appropriate for determining the species
216 specific value of $v_{t,i}$ for species i . However, given the large number of possible species of
217 interest, and the effort required to find a suitable analytical method for measuring local
218 flux for each species, it is more fruitful to find a way to measure a species independent
219 parameter that can be used to determine $v_{t,i}$. To this end, Morrison et al. (2003) argues for
220 the use of a species-independent parameter, the friction velocity, that allows indoor
221 emission/deposition rate measurements for one species, j , to be used to determine $v_{t,i}$ for
222 any other gas phase species, i . This parameter can then be used as a reporting metric
223 which allows results based on a variety of methodologies to be compared in the most
224 consistent manner.

225 An alternative to the use of the friction velocity as a species independent reporting
226 metric is to report the mass-transfer coefficient for a representative species at a standard
227 temperature. For example, since indoor ozone exposures are of great interest for
228 understanding ambient pollution induced health problems, indoor/outdoor concentrations
229 have been quantified extensively (Weschler et al., 1994). In addition, ozone deposition
230 rate measurements have been derived directly (Morrison et al., 2003), indirectly
231 (Weschler et al., 1989) or inferred (Cano-Ruiz et al., 1993). Given the broad interest in
232 ozone and the fact that an analytical technique (Morrison et al., 2003) already exists for
233 measuring ozone flux to surfaces, this is a suitable candidate for “representative species”,
234 as recognized by Cano-Ruiz et al. (1993).

235 Converting this value for ozone, $v_{t,ozone}$, to that for any other species requires that
236 the conversion is independent of fluid flow conditions. Fortunately, correlations exist for
237 both laminar and turbulent mass-transfer coefficients in a variety of settings. For most

238 fluid-mechanical systems, the mass-transfer coefficient, $v_{t,i}$, is proportional to $D_i^{-0.67}$. This
239 concept holds for transport through boundary layers in general. Therefore, only the
240 diffusion coefficients respectively for ozone and species i , D_{ozone} , D_i , are required to carry
241 out the conversion:

$$242 \quad v_{t,i} = v_{t,ozone} \left(\frac{D_{ozone}}{D_i} \right)^{0.67} \quad (15)$$

243 A simplifying advantage of this method, over reporting friction velocity, is that diffusion
244 coefficients are already tabulated (Massman, 1998) or can be easily estimated for most
245 gaseous species (Baum, 1998). Reporting mass transfer conditions in terms of $v_{t,ozone}$ does
246 not preclude measurements using other species; the results are merely reported in terms
247 of ozone. The natural extension of this idea is that even non-pollutants, such as water,
248 could be used to measure mass-transport conditions, which are then reported as $v_{t,ozone}$.
249 Thus, deposition velocity results that we derive from octadecane emission rate
250 measurements are reported as $v_{t,ozone}$.

251

252 **3. Methods**

253

254 *3.1 Deviation of measured from actual time-averaged v_t : simulations*

255

256 To demonstrate the extent to which this method erroneously evaluates the average
257 deposition velocity, it is useful to compare the measured time-average $\bar{v}_{t,measured}(s)$ with
258 the “actual” value $\bar{v}_{t,actual}(s)$ under changing conditions in a model building. First define
259 the following ratio of $\bar{v}_{t,measured}$ to $\bar{v}_{t,actual}$:

$$f_t = \frac{\bar{v}_{t,measured}(s)}{\bar{v}_{t,actual}(s)} = \frac{(t_2 - t_1) \int_{t_1}^{t_2} v_t(s,t) C_b(s,t) dt}{\int_{t_1}^{t_2} C_b(s,t) dt \int_{t_1}^{t_2} v_t(s,t) dt} \quad (16)$$

261 If, in this simulation, f_t deviates significantly from unity, the time-averaged measurement
 262 is shown to be in error. For the sake of brevity, the parenthetical (s) is omitted in this
 263 section and each variable is independent of location s .

264 Applying a mass-conservation model to an indoor volume acting as a well mixed
 265 reactor, the dynamic indoor concentration, C_b , of a surface-reactive pollutant without
 266 indoor sources is represented by

$$\frac{dC_b(t)}{dt} = \lambda C_o - \lambda C_b(t) - \frac{A v_d(t) C_b(t)}{V} \quad (17)$$

268 where λ is the air-exchange rate for the building (Q/V) and v_d transport-limited
 269 deposition velocity defined by Eq. (2). Note again that the concentration and the
 270 deposition velocities are coupled quantities in the last term of Eq. (17).

271 There are numerous ways to drive the function, Eq. (17), so that the influence of
 272 changing conditions on the measurement can be evaluated. For simplicity, the following
 273 conditions are fixed: λ , C_o , A , and V . Only the deposition velocity will change, reflecting
 274 changing internal conditions of the building such as periodic operation of recirculation in
 275 a residence which has a minimal effect on ventilation rate, and differences in the surface
 276 reaction probability, γ , which is held constant for each simulation. Values chosen for this
 277 analysis are: $\lambda = 0.5 \text{ h}^{-1}$, $A/V = 2 \text{ m}^{-1}$, total time interval = 12 h. The transport-limited
 278 deposition velocity is forced to follow a sinusoidal functional form, and as a result the
 279 range, or amplitude, of deposition velocity values and the sinusoidal period can be

280 adjusted to cover a wide range of prototypical situations, e.g. fast or slow cycling of a
281 recirculation system. The sinusoidal form of v_t is defined as follows:

$$282 \quad v_t = \left(\frac{v_{t,max} + v_{t,min}}{2} \right) + \left(\frac{v_{t,max} - v_{t,min}}{2} \right) \sin\left(\frac{\pi}{6} c \cdot t \right) \quad (18)$$

283 where $v_{t,max}$ and $v_{t,min}$ are respectively the maximum and minimum extents of v_t , c is the
284 number of sinusoidal cycles per 12 hour period (h^{-1}) and t is the elapsed time (h). The
285 parameters $v_{t,max}$ and $v_{t,min}$ are constant for a given simulation, but cover a range from 0.05
286 to 0.5 cm s^{-1} for a variety of simulations.

287

288 3.2 Deviation of measured from actual time-averaged v_t : DeVS measurements

289

290 It remains to be seen how much *typical* indoor conditions change and by what
291 extent they may change over typical averaging periods. Using a deposition velocity
292 sensor, or DeVS, for measuring *instantaneous* values of v_t , we observed the anticipated
293 range of values of $v_{t,ozone}$ over typical 2-8 hour periods in mechanically ventilated rooms.
294 Briefly, a 1-cm diameter quartz-crystal microbalance was placed on a room surface,
295 coated with octadecane and the rate of change of mass on the sensor was observed as the
296 octadecane evaporated into the room. The local, instantaneous value of $v_t(s,t)$ was then
297 evaluated from the flux, $J(s,t)$, derived directly from this measurement, and $C_s(s,t)$ is
298 derived from the octadecane vapor pressure. Details of this method can be found in
299 (Morrison et al., 2003). The resulting values of $v_t(s,t)$ for octadecane are converted and
300 reported as $v_{t,ozone}$, consistent with the reporting metric recommended in section 2.3.
301 Temporal variability in $v_{t,ozone}$ was evaluated by introducing realistic changes in activity
302 or ventilation. In room 1, a residential laundry room, changes were introduced by turning

303 on and off a ceiling mounted ventilation fan with a period of approximately 1 hour. In
304 room 2, an office, changes were introduced by changing the number of occupants, their
305 activity and by opening a window (details in Morrison et al. (2003)). Combined with this
306 real-time data, Eq. 15 is used to simulate the ratio of indoor to outdoor concentrations of
307 ozone (C_{in}/C_{out}) for two different reaction probability values (a typical value for ozone, γ
308 = 10^{-5} , and a limiting high value, $\gamma = 1$).

309

310 **4. Results**

311

312 The results of the simulations outlined in section 3.1 are shown in Figs. 1a, 1b and
313 1c. Fig. 1a shows how the deposition velocity ratio, f_t (Eq. (15)), is influenced by the
314 high-low ratio, ($v_{t,max}/v_{t,min}$), where the sinusoid experiences a single cycle over a 12 h
315 period. Here, γ is held at 1 and the number of cycles is held equal to 1. Also shown for
316 two points along the curve are 12 h simulations of C_{in}/C_{out} and v_t . The primary
317 observation is that for a large change in the deposition velocity over the time interval, a
318 time-integrated deposition measurement method under-predicts $\bar{v}_{t,ozone}$ substantially. For
319 the widest range of deposition velocities anticipated indoors ($v_{t,max}/v_{t,min} = 10$), time-
320 integrated methods under-predict by about 40%. However, the under-prediction is most
321 substantial for a very large range of indoor conditions. If the range is somewhat more
322 modest (e.g. $v_{t,max}/v_{t,min} = 3$), the under-prediction is about 10%, which is of the same
323 order of magnitude as the measurement uncertainty of the time-averaging method
324 employed by Morrison et al. (2003) for ozone deposition measurements. The ratio f_t

325 appears to be insensitive to the actual values of $v_{t,max}$ and $v_{t,min}$. For example, $f_t = 0.95$ for
326 $(v_{t,max}/v_{t,min}) = 2$ whether $v_{t,max} = 0.1$ and $v_{t,min} = 0.05$, or $v_{t,max} = 0.5$ and $v_{t,min} = 0.25$.

327 Fig. 1b demonstrates how the number of sinusoidal cycles influences the
328 measurement error of a time-averaging method. Again, this sinusoidal variability can be
329 likened to periodic changes to the indoor environment due to central heating fans turning
330 on and off. Here, $v_{t,high}/v_{t,low}$ is held at 10 and γ is held at 1. For a slowly changing value
331 of the deposition velocity, the error is small ($\sim 5\%$), but for anything greater than a single
332 cycle over the averaging period, the maximum error is obtained. For mechanical
333 ventilation/recirculation, the maximum error would occur for most indoor measurements.

334 Fig. 1c demonstrates how the reaction probability of indoor surfaces will
335 influence a time-averaged measurement for measured pollutants such as O_3 or NO_2 . Here,
336 $v_{t,max}/v_{t,min}$ is held at 10 and the number of cycles is held equal to 1. As the reaction
337 probability increases, the influence of surfaces on the resulting indoor concentration
338 increases. Consequently, f_t decreases and the measurement error increases. The greatest
339 error is incurred when trying to use the most surface reactive pollutants such as acids,
340 radicals and aerosols to measure deposition flux. For a pollutant such as ozone, the mean
341 surface reaction probability, γ , lies between 10^{-7} and 10^{-4} (Cano-Ruiz et al., 1993;
342 Morrison and Nazaroff, 2000; Reiss et al., 1995) and the error increases from ~ 0 to 40%
343 over that range of γ . For time-averaged measurements of v_t , a species that reacts poorly
344 with indoor surfaces would appear to be preferable. However, spatial considerations
345 discussed in a separate article (Morrison and Zhao, 2005) weaken this finding.

346 Fig. 2a shows the results of a DeVs measurement in a room in which an exhaust
347 fan is turned on and off with a period of about 1 hour. The transport-limited deposition

348 velocity is reported as ozone, $v_{t,ozone}$, even though the measurement is based on
349 octadecane emission flux from a microbalance (see Section 2.3). Eq. 16 is used to
350 simulate the ratio of indoor to outdoor concentrations of ozone (C_{in}/C_{out}) for two different
351 reaction probability values (a typical value for ozone, $\gamma = 10^{-5}$, and a limiting high value,
352 $\gamma = 1$) and the results are shown in Figure 2a as dashed lines. As $v_{t,ozone}$ increases and
353 decreases, the indoor concentration of ozone decreases and increases respectively as
354 anticipated. The value of $(v_{t,max}/v_{t,min})$ is ~ 3 and the number of cycles is ~ 4 . The value f_i
355 shown in Fig 2a is determined using Eq. (14) and Eq. (15). For a typical reaction
356 probability of ozone, the error is small (1%); where the reaction probability is large (e.g.
357 for acid gases), the error would be higher but not substantial (5%). A second field
358 measurement is shown in Fig 2b along with simulated pollutant concentrations. The
359 regions of low and high $v_{t,ozone}$ are due to changes in activity in an office (room 2). In this
360 case, an error of 20% would be incurred if a highly surface-reactive species is used to
361 measure v_t .

362 5. Discussion

363 The results point to systematic error in relying on time-averaged methods to
364 determine indoor mass-transfer coefficients. For many cases, this may be minor or even
365 negligible. Yet these errors cannot be ignored until more data on indoor transport
366 variability is generated. Measurements using a highly surface reactive species, such as
367 nitric acid, incur the greatest error for infiltrated pollutants. The measurement error
368 incurred for species that are moderately surface reactive, such as ozone, varies depending
369 on the type of surfaces available for deposition.

370 The simulations suggest that there is an advantage to using a species with a low
371 reaction probability, or little tendency to react with indoor surfaces. However, this is only
372 true for species transported indoors that adhere to the assumptions underlying the
373 simulations. The reason f_t tends to be less than 1 in simulations for surface reactive
374 species is because of the inverse correlation between concentration and v_t : as v_t increases,
375 surface reactive pollutant concentrations decrease. If CO₂ were used, instead, for time-
376 averaged deposition measurements (e.g. to a filter coated with LiOH), a positive
377 correlation is probable, even though CO₂ will not be significantly consumed by indoor
378 surfaces. As building occupancy increases, CO₂ concentrations and the intensity of air
379 movement increases. This will result in $f_t > 1$ if the measurement period covers both
380 occupied and unoccupied times. It may be advantageous, in this case, to choose the
381 averaging time to coincide with a period in which CO₂ concentrations are relatively
382 steady, i.e. during the middle of the work day or overnight. Thus, the species used for
383 deposition measurements influences the choice of sampling time periods. Note that, while
384 the deposition velocity of CO₂ itself is not of interest in indoor pollutant modeling, the
385 mass-transfer coefficients obtained using this species can be converted to that for any
386 other gaseous species by Eq. 15.

387 The value of f_t can be generated with knowledge of the system in use. Eq. 16,
388 defining f_t , can be used as long as continuous methods of measuring $v_t(t)$ and $C(t)$ are
389 being used in conjunction with time-averaged methods. From this value, the time-
390 averaged methods can be corrected using,

391
$$\bar{v}_{t,corrected} = \frac{\bar{v}_t}{f_t} \quad (19)$$

392 A further correction is required to account for the size of the device used to make the
393 time-averaged measurement of v_t (Morrison and Zhao, 2005), but will not be discussed
394 here.

395 In these analyses, we have ignored the short-time influences of changing
396 conditions. In an earlier example, ozone concentration and fluid momentum increases
397 indoors due to increased ventilation through a window. There is an inherent lag-time
398 between the increased momentum and increased transport conditions at the surface. The
399 time for momentum changes to propagate through the boundary layer can be roughly
400 estimated by dividing the typical indoor boundary layer thickness, ~ 1 cm, by a typical
401 mass-transfer coefficient for N_2 , ~ 0.1 cm s^{-1} , to arrive at a transition time of ~ 10 s. A
402 continuous measurement device, at an indoor surface, may not reliably account for
403 changes that occur on these time scales, even if it responds at faster time-scales. For
404 example, the DeVVS device has a response time of approximately 1-10 seconds. Since
405 overall mixing time-scales in rooms are of the order of minutes, this boundary-layer lag
406 time may not be important, but should be examined further.

407 Given the error inherent in time-averaged measurements, instantaneous methods
408 are preferred. To date, only the DeVVS system of Morrison et al. (2003) appears to meet
409 the criteria of being a true mass-transfer sensor, instantaneous (second to minute scale)
410 and local (centimeter spatial scale); see Figs. 2a and 2b for example results. Similar
411 devices can be envisioned that employ evaporation or deposition and an appropriate
412 transducer to convert surface mass change into an electronic signal. For example, Black
413 et al. (Black et al., 2000) developed a microbalance based ozone concentration sensor that
414 quantified the rate of oxidation of an unsaturated organic polymer coating. Because

415 concentration was the endpoint, they maintained the sensor in a controlled air stream to
416 keep the boundary mass-transfer resistance constant. However, positioning the coated
417 microbalance on an indoor surface and quantifying the rate of mass change due to ozone
418 uptake would provide information sufficient to determine a local and instantaneous value
419 of $v_{t, \text{ozone}}$. Other possible direct mass-flux methods could include: CO₂ uptake on LiOH,
420 H₂O uptake on silica gel or H₂O evaporation rate.

421

422 **6. Conclusions**

423

424 Although using time-averaged deposition of an existing surface-reactive pollutant
425 as a method of finding v_t is limiting, it remains to be seen just how poor this choice will
426 be for wide-spread measurements. If the bulk-room concentration, \bar{C}_b , can be maintained
427 roughly constant, then time-averaged flux measurements should work well. These kinds
428 of measurements are most suitable when attempting to derive a spatial distribution of
429 transport in buildings because they are easily deployed in large numbers (e.g. coated
430 filters distributed across a wall). Further information is needed to determine the extent to
431 which changing conditions influence time-averaged measurements.

432 The measurement accuracy of heat and mass-transfer coefficients in practice is
433 limited. Even carefully controlled conditions in model systems (e.g. duct), result in
434 correlations that are no better than 30 percent (Kreith, 1973). Yet, the error predictions
435 reported here are systematic errors, shifting the median value among a collection of
436 measurements. Recognition of these errors is imperative, especially this early in our
437 understanding of indoor transport phenomena. Error associated with the use of a time-

438 averaging flux measurement may be modest for most indoor environments. The
439 maximum error predicted here (~40%) occurs when the mass-transfer coefficient varies
440 by one order of magnitude during the averaging period. This may be unusual for most
441 indoor systems and time-averaging methods may provide good values with only a small
442 systematic error. More observations of the dynamics of mass-transfer coefficients in
443 indoor environments are necessary to proceed further with time-averaged measurements.

444

445 **Acknowledgements**

446

447 This material is based upon work supported by the National Science Foundation under
448 Grant No. 0238721. We thank Ping Zhao for her help with initial calculations, Priscilla
449 Morrison for significantly improving the manuscript and the folks from the UMR pre-
450 tenure writer's group for their suggestions.

451

452 **References**

453 Baum, E. J. 1998. Chemical property estimation theory and practice. Boca Raton, FL,
454 Lewis Publishers.

455

456 Black, D. R., Harley, R. A., Hering, S. V. 2000. A new, portable, real-time ozone
457 monitor. *Environmental Science & Technology* 34(14): 3031-3040.

458

459 Cano-Ruiz, J. A., Kong, D., Balas, R. B., Nazaroff, W. W. 1993. Removal of reactive
460 gases at indoor surfaces: Combining mass transport and surface kinetics. *Atmospheric*
461 *Environment* 27a: 2039-2050.

462

463 Gadgil, A. J., Lobscheid, C., Abadie, M. O., Finlayson, E. U. 2003. Indoor pollutant
464 mixing time in an isothermal closed room: An investigation using cfd. *Atmospheric*
465 *Environment* 37(39-40): 5577-5586.

466

467 Kreith, F. 1973. Principles of heat transfer. New York and London, Intext Educational
468 Publishers.

- 469
470 Massman, M. J. 1998. A review of the molecular diffusivities of h₂o, co₂, ch₄, o₃, so₂,
471 nh₃, n₂o, no, and no₂ in air, o₂ and n₂ near stp. *Atmospheric Environment* 32(6): 1111-
472 1127.
- 473
474 Morrison, G. C., Nazaroff, W. W. 2000. The rate of ozone uptake on carpets:
475 Experimental studies. *Environmental Science & Technology* 34(23): 4963-4968.
- 476
477 Morrison, G. C., Zhao, P. 2005. Spatial considerations in the measurement of indoor
478 mass transfer coefficients. *Atmospheric Environment* in submission.
- 479
480 Morrison, G. C., Zhao, P., Wiseman, D. J., Ongwandee, M., Chang, H., Portman, J.,
481 Regmi, S. 2003. Rapid measurement of indoor mass-transfer coefficients. *Atmospheric*
482 *Environment* 37: 5611-5619.
- 483
484 Nazaroff, W. W., Cass, G. 1987. Particle deposition from a natural convection flow onto
485 a vertical isothermal flat plate. *Journal of Aerosol Science* 18(4): 445-455.
- 486
487 Nazaroff, W. W., Gadgil, A. J., Weschler, C. J. 1993. Critique of the use of deposition
488 velocity in modeling indoor air quality. Berkeley, CA, Civil Engineering Department,
489 University of California: 81-103.
- 490
491 Reiss, R., Ryan, P. B., Tibbetts, S. 1995. Ozone reactive chemistry on interior latex paint.
492 *Environmental Science & Technology* 29: 1906-1912.
- 493
494 Salmon, L., Nazaroff, W. W., Ligocki, M. P., Jones, M., Cass, G. 1990. Nitric acid
495 concentration in southern california museums. *Environmental Science & Technology*
496 24(7): 1004-1013.
- 497
498 Thatcher, T. L., Nazaroff, W. W. 1997. Effect of small-scale obstructions and surface
499 textures on particle deposition from natural convection flow. *Aerosol Science and*
500 *Technology* 27: 709-725.
- 501
502 Weschler, C. J., Shields, H., Naik, D. V. 1989. Indoor ozone exposures. *JAPCA: Journal*
503 *of the Air and Waste Management Association* 39: 1562-1568.
- 504
505 Weschler, C. J., Shields, H. C., Naik, D. V. 1994. Indoor chemistry involving o₃, no, and
506 no₂ as evidenced by 14 months of measurements at a site in southern california.
507 *Environmental Science & Technology* 28(12): 2120-2132.
- 508

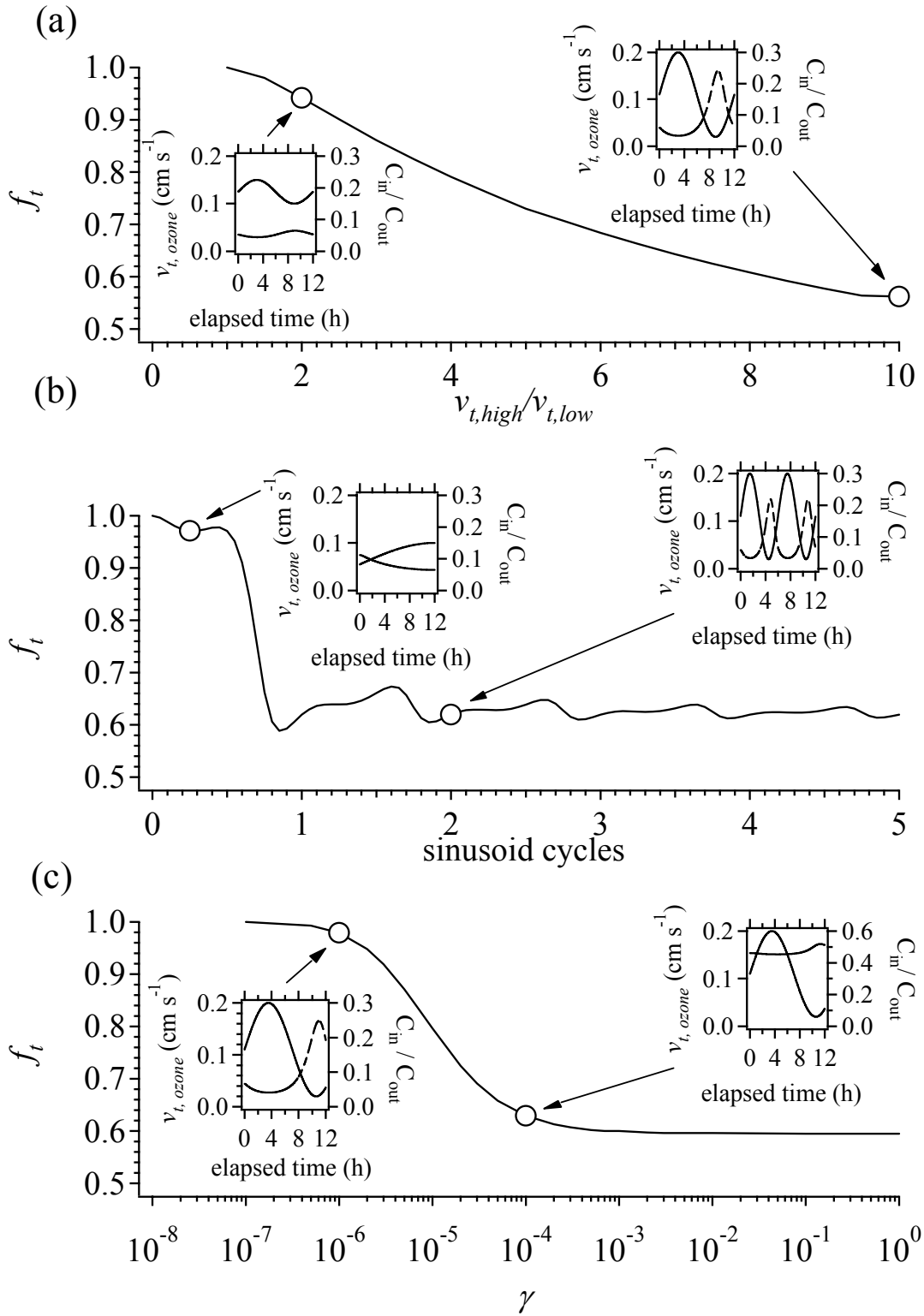
509 **Figure and Table Captions**

510

511 **Fig. 1.** Ratio, f_t , of $\bar{v}_{t,measured}$ to $\bar{v}_{t,actual}$ for a variety of temporally changing conditions: a)
512 influence of the range of values, characterized by the ratio, $v_{t,high}/v_{t,low}$ b) influence of
513 sinusoid frequency, c) influence of surface reaction probability, γ . Solid traces
514 corresponds to left-hand axes, dashed traces correspond to right-hand axes.

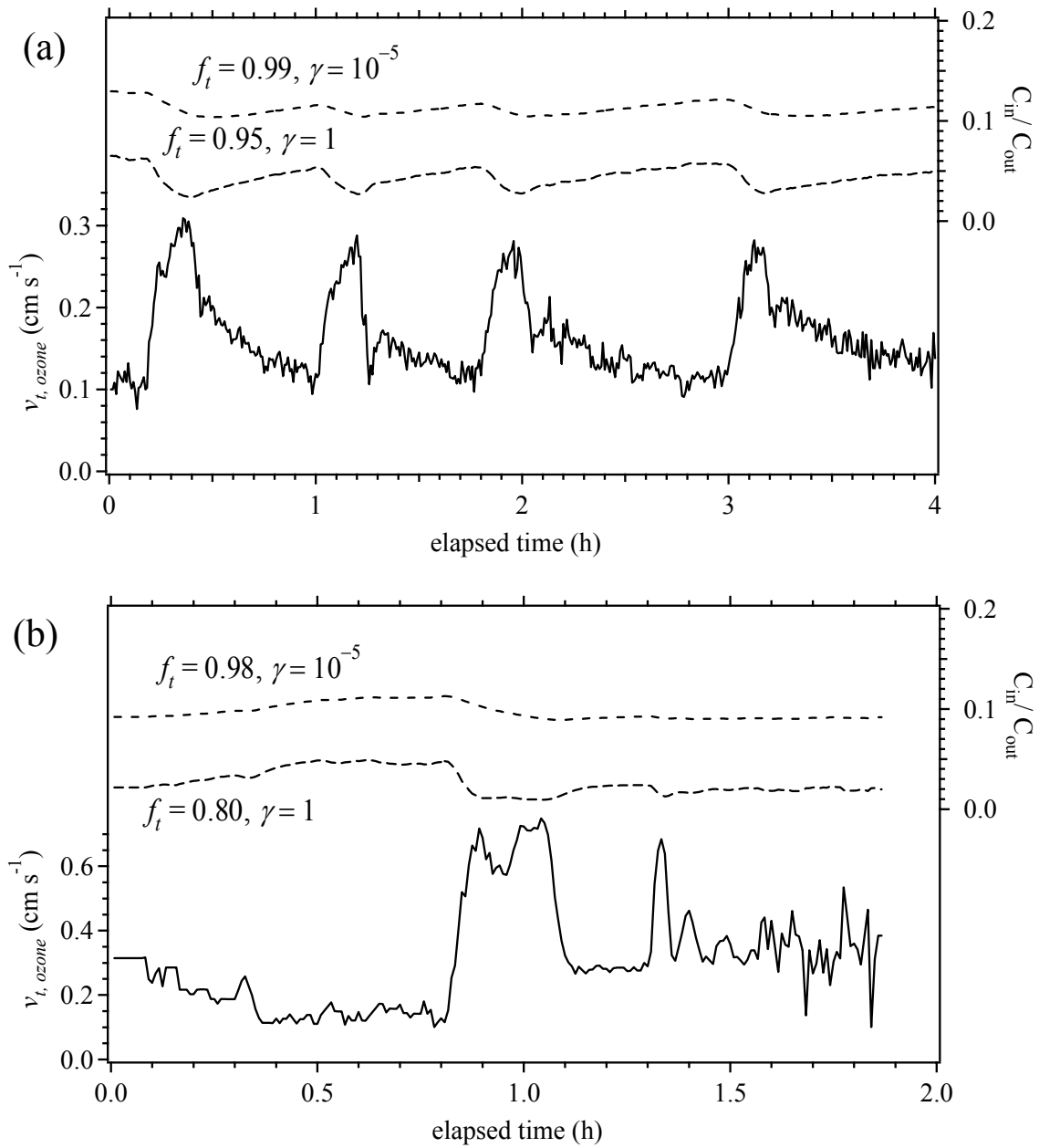
515 **Fig. 2.** Mass-transport limited deposition velocity, $v_{t,ozone}$, reported “as ozone” and
516 simulated indoor ozone concentrations for two field measurements using a continuous
517 microbalance flux measurement (Morrison et al., 2003): (a) a 4-h measurement in a room
518 in which an exhaust fan is turned on and off on a ~ 1 hour cycle; (b) a 2-h measurement
519 in an office with varying levels of occupant activity. For two different values of the
520 reaction probability, γ , the ratio f_t is calculated.

521 **Figure 1**



522

523 **Figure 2**



524

525

526

527

528 **Nomenclature**

529

530	A	superficial exposed surface area of a room (m^2)
531	C	sinusoidal cycles in a 12 hour simulation (cycles)
532	C_b	concentration at the outer edge of the concentration boundary layer, or
533		core room concentration, ($\mu g\ m^{-3}$)
534	\bar{C}_b	steady-state, volume averaged core concentration ($\mu g\ m^{-3}$)
535	C_o	outdoor concentration ($\mu g\ m^{-3}$)
536	\bar{C}_{O_3}	time and volume-averaged room concentration of ozone during the
537		exposure interval ($\mu g\ m^{-3}$)
538	C_s	near-surface gas concentration of the pollutant ($\mu g\ m^{-3}$)
539	D	diffusion coefficient ($m^2\ s^{-1}$)
540	f_t	ratio of measured, $\bar{v}_{t,measured}$, to actual, $\bar{v}_{t,actual}$, time-averaged, transport
541		limited deposition velocity (dimensionless)
542	J	flux to or from surface ($\mu g\ m^{-2}\ s^{-1}$)
543	\bar{J}	time-average flux to or from surface ($\mu g\ m^{-2}\ s^{-1}$)
544	m_{NO_3}	mass of nitrate formed on a DeVO filter (g),
545	MW	molecular weight of the subscripted compound ($g\ mol^{-1}$)
546	Q	infiltration rate ($m^3\ s^{-1}$)
547	s	surface location (m,m)
548	t	time (s)
549	Δt	time interval exposed (h or s)
550	V	volume of a room (m^3)
551	$\langle v \rangle$	Boltzman's velocity ($m\ s^{-1}$)
552	v_d	apparent deposition velocity ($m\ s^{-1}$)
553	v_t	transport-limited deposition velocity ($m\ s^{-1}$)
554	\bar{v}_t	time-averaged, transport-limited deposition velocity ($m\ s^{-1}$)
555	$\bar{v}_{t,ozone}$	time-averaged, transport-limited deposition velocity for ozone ($m\ s^{-1}$)
556	$v_{t,max}$	maximum extent of v_t for simulations ($m\ s^{-1}$)
557	$v_{t,min}$	minimum extents of v_t for simulations ($m\ s^{-1}$)
558	$\bar{v}_{t,measured}$	measured, time-averaged, transport-limited deposition velocity ($m\ s^{-1}$)
559	$\bar{v}_{t,actual}$	actual, time-averaged, transport limited deposition velocity($m\ s^{-1}$)
560	γ	species (e.g. ozone) reaction probability with surface (dimensionless)
561	λ	air-exchange rate for the building (s^{-1})
562		
563		